Video Article

Cerenkov Luminescence Imaging of Interscapular Brown Adipose Tissue

Xueli Zhang[1,2], Chaincy Kuo[3], Anna Moore[1], Chongzhao Ran[1]

[1]Molecular Imaging Laboratory, MGH/MIT/HMS Athinoula A. Martinos Center for Biomedical Imaging, Department of Radiology, Massachusetts General Hospital/ Harvard Medical School

[2]Center for Drug Discovery, School of Pharmacy, China Pharmaceutical University

[3]Perkin Elmer

Correspondence to: Chongzhao Ran at cran@nmr.mgh.harvard.edu

URL: https://www.jove.com/video/51790
DOI: doi:10.3791/51790

Keywords: Medicine, Issue 92, Cerenkov luminescence imaging, brown adipose tissue, 18F-FDG, optical imaging, *in vivo* imaging, spectral unmixing

Date Published: 10/7/2014

Citation: Zhang, X., Kuo, C., Moore, A., Ran, C. Cerenkov Luminescence Imaging of Interscapular Brown Adipose Tissue. *J. Vis. Exp.* (92), e51790, doi:10.3791/51790 (2014).

Abstract

Brown adipose tissue (BAT), widely known as a “good fat” plays pivotal roles for thermogenesis in mammals. This special tissue is closely related to metabolism and energy expenditure, and its dysfunction is one important contributor for obesity and diabetes. Contrary to previous belief, recent PET/CT imaging studies indicated the BAT depots are still present in human adults. PET imaging clearly shows that BAT has considerably high uptake of ^{18}F-FDG under certain conditions. In this video report, we demonstrate that Cerenkov luminescence imaging (CLI) with ^{18}F-FDG can be used to optically image BAT in small animals. BAT activation is observed after intraperitoneal injection of norepinephrine (NE) and cold treatment, and depression of BAT is induced by long anesthesia. Using multiple-filter Cerenkov luminescence imaging, spectral unmixing and 3D imaging reconstruction are demonstrated. Our results suggest that CLI with ^{18}F-FDG is a practical technique for imaging BAT in small animals, and this technique can be used as a cheap, fast, and alternative imaging tool for BAT research.

Video Link

The video component of this article can be found at https://www.jove.com/video/51790/

Introduction

Brown adipose Tissue (BAT) is a special tissue for thermogenesis in mammals, and one of its major functions is to maintain the energy balance of the whole body through dissipating large amounts of chemical/food energy as heat [1]. BAT's most unique characteristics include plentiful uncoupling protein-1 (UCP-1) expression, abundant small oil droplets, a large number of mitochondria in a single cell, and significant vascularization in the tissue [2-5]. These unique features strongly associate with the tissue's important role in metabolism and energy expenditure. BAT was previously considered to be no longer present and possessing no significant physiological functions in adult humans [1], however recent PET/CT imaging investigations have clearly demonstrated that BAT still presents in human adults [2,3,6-9]. An inverse correlation between BAT mass and body mass index (BMI) was established from several studies, and recent studies indicated that physical exercises could increase the mass of BAT. These results strongly suggest that the dysfunction of BAT is tightly associated with the pathologies of obesity and diabetes [2,6,10,11]. In addition, mounting evidence indicates that the function of BAT is strongly related to various other pathologies such as neurodegenerative disease and cancer [3,7,12,13].

BAT activation, a process to increase thermogenesis, can be achieved under various conditions such as cold exposure, exercise, and drug treatment and gene manipulation [1,14,15]. Cold exposure and norepinephrine treatment are the most used methods to activate BAT. Cold, which can be sensed by various mechanisms such as thermoreceptors in the skin, stimulates sympathetic nerves and leads to the release of norepinephrine (NE) to BAT. The released NE triggers UCP-1 to initialize thermogenesis to maintain the normal body temperature. Under this condition, the uptake of glucose also increases to provide more carbon sources for the increased metabolism in BAT [1,16,17]. PET imaging with 18F-FDG has confirmed that the uptake of labeled glucose increased under cold conditions in human studies [6].

In terms of optical imaging, BAT is an ideal target. The interscapular BAT has a unique location in mice, situated away from larger organs such as the liver, heart, and stomach. Therefore, signal interference from these large organs is insignificant (**Figure 1a**). Meanwhile, the shallow location of interscapular BAT allows more signals to be captured by the detection camera. Moreover, BAT is a concentrated mass organ, which confines the light signal in certain areas. Additionally, the unique triangular physical shape of BAT makes it easy to distinguish from other tissues (**Figure 1a**).

Cerenkov luminescence imaging (CLI), a newly emerged molecular imaging technology [18-26], harnesses the luminescence generated from the $^{+}$ and $^{-}$ decay of radionuclides such as ^{18}F and ^{131}I in the medium. The charged particle (such as $^{+}$ and $^{-}$) polarizes molecules while it travels in the medium [18-20], and luminescence/light is emitted when the polarized molecules relax back to equilibrium. The emitted luminescence is called Cerenkov Luminescence (CL). The unique spectral properties of CL include its broad spectrum throughout the ultraviolet (UV) and visible spectrum [18-20], and its inverse correlation between the intensity and the square of the wavelength (λ^2). Both UV and visible ranges of the emitted

light can be utilized for different applications. The UV portion of Cerenkov luminescence has been applied for *in vivo* photoactivation of caged luciferin [21], while the light emitted in the longer wavelength can be used for *in vivo* optical imaging [18,27-31].

For small animal studies, CLI imaging with an optical imaging system is faster and more cost effective than PET. Moreover, CLI can be applied for high throughput screening with an imaging system equipped with high throughput capacity. The advantages and disadvantages of this technology have been discussed in several reviews [25,32,33]. 3D tomography of CLI has been intensively studied in several groups [28,34-37], and the applications of CLI for endoscopic imaging and intraoperative imaging have been successfully demonstrated in mice as well [30,38]. In addition, Spinelli and Thorek *et al.* have demonstrated that CLI imaging could be applied to human subjects, thus the technology also has potential for clinical applications [39,40].

In the course of rediscovery of BAT in humans, PET images clearly indicated that a significant amount of ^{18}F-FDG accumulated in BAT under certain conditions [2,3,6]. In addition, PET imaging with mice also undoubtedly showed that BAT could be highlighted with ^{18}F-FDG [4142]. In this report, we demonstrate how Cerenkov luminescence emitted from ^{18}F-FDG can be utilized for imaging BAT in small animals using an optical imaging system. Our approach provides a fast, cheap and convenient method of BAT imaging for small animals. This technique can be used as an alternative method for PET imaging with ^{18}F-FDG, especially for laboratories without PET facilities.

Protocol

Note: All animal studies should be performed under approved institutional protocols and animal care guidelines.

1. *In Vivo* CLI imaging BAT with ^{18}F-FDG

1.1 Background Imaging:

1. Before ^{18}F-FDG injection, place four nude mice in an induction chamber that has been connected with isoflurane balanced with oxygen for 5 min to induce anesthesia. Then place the four anesthetized mice into the imaging apparatus.
2. Acquire the background image with the following parameters: Open filter, f = 1, bin = 8, FOV = D, and exposure time = 120 sec, stage temperature = 37 °C.

1.2 BAT Imaging with ^{18}F-FGD:

1. Inject the anesthetized mice with 280 µCi of ^{18}F-FDG in PBS intravenously in the tail vein. After the injection, return the mice to a cage equipped with food and water.
   Note: It is necessary to intravenously inject ^{18}F-FDG to achieve a decent contrast around BAT area. Only a very weak contrast can be seen with the same amount of ^{18}F-FDG if an intraperitoneal injection is used.
2. Acquire CLI images at 30, 60, and 120 min after ^{18}F-FDG injection with the same parameters as background imaging (step 1.1.2). For each imaging session, allow 5 min for the anesthesia reinduction.
3. To quantify the signal to noise ratio (S/N), use the imaging software interface to draw two equal sized ellipse ROIs over the interscapular BAT and an area adjacent to the BAT (reference area) (**Figure 1b**).

1.3 Validation of the CLI Source:

1. Anesthetize four mice and inject the mice with 280 µCi of ^{18}F-FDG intravenously.
2. Sacrifice the mice 60 min after the injection of ^{18}F-FDG by injection of sodium pentobarbital (200 mg/kg, IP). Carefully remove the skin from the interscapular area. Image all of the mice with the same parameters as above (1.1.2), at the same time (**Figure 2a**).
3. Carefully remove the interscapular white adipose tissue (WAT) and BAT, and then image the dissected mice with the same parameters (**Figure 2b**).
4. From the CLI images, calculate the contribution from BAT by using two ROIs with the following equation: $R_{(BAT)} = (CLI_a\text{-}CLI_b)_{(BAT)}/(CLI_a\text{-}CLI_b)_{(BAT\text{-}removed)}$, where ROI_a is for the interscapular area and ROI_b is for the reference area (**Figure 2b**).

2. BAT Imaging Application

2.1 Monitoring Activation with NE

1. Divide nude mice into two groups (n = 4 each).
2. Inject one group with norepinephrine (NE) (50 µl, 10mM) intraperitoneally. Use the second group as a non-activated control. After 30 min, anesthetize both groups with isoflurane for 5 min, and then intravenously inject each mouse with ^{18}F-FDG (220 µCi).
   Note: The intraperitoneal injection of NE should be 30 min before ^{18}F-FDG injection to avoid dramatically agitating the mice.
3. Image the mice 60 min after ^{18}F-FDG injection using the same parameters as the above protocols.

2.2 Monitoring Activation Under Cold Exposure

1. Measure the body temperatures of the mice in the cold room with a rectal thermometer. Temperatures should be about 30 °C.
2. Image the mice 60 min after ^{18}F-FDG injection by using the same imaging parameters as the above protocols. Use mice that are kept at room temperature (25 °C) as the controls, and image them with the same.
3. For a cold exposure study, place the mice in a cold room (4 °C) for 4 hr before ^{18}F-FDG injection and return the mice to the cold room after each imaging session and after recovering from anesthesia.
4. parameters as above.

2.3 Monitoring Deactivation of BAT Under Long Anesthesia

1. For long anesthesia (60 - 70 min), inject mice intraperitoneally with ketamine/xylazine and keep them under anesthesia for 60 - 70 min at room temperature.
2. Once the mice are anesthetized, inject ^{18}F-FDG (220 µCi) intravenously via the tail vein.
3. Image the mice 60 min after ^{18}F-FDG injection by using the same parameters as the above protocols.

3. Spectral Unmixing and Multispectral Cerenkov Luminescence Tomography Studies

1. Anesthetize a mouse for 5 min, and then inject 300 µCi ^{18}F-FDG intravenously. Acquire multispectral images 60 min after ^{18}F-FDG injection from the animal's dorsal side with the following parameters: f = 1, bin = 16, acquisition time = 300 sec per filter, emission filters = 580, 600, 620, 640, 660 and 680 nm.
2. Conduct spectral unmixing with Living Imaging 4.3.1 software and select two components (BAT and unspecific signals) and automatic unmixing (**Figure 4**).
3. Conduct the 3D reconstruction according to the method reported by Kuo *et al*. [28,43]. Incorporate the Cerenkov emission spectrum into the diffuse light propagation model, apply Tikhonov regularization in the NNLS (nonnegative least squares) optimization of the residuals, and generate the surface tomography (which is used for 3D image coregistration) from the structure light imaging (**Figure 5**).
   Note: For multispectral CLI spectral unmixing and tomography, at least 5 images with different filters are needed.

Representative Results

In **Figure 1**, interscapular BAT (**Figure 1a**) was highlighted at all time points (30, 60, 120 min), and the contrast between BAT and the reference area can be easily observed (**Figure 1b**). Notably, the contour of the BAT image closely reflected its physical appearance, which has a triangular contour. The signal ratios between BAT and the reference area were 2.37, 2.49, and 2.53 fold at 30, 60, and 120 min after injection (**Figure 1a**).

From the step-wise dissection experiment, 85% of the signal at the interscapular site had originated from the BAT (**Figure 2**). However, there was still some residual signal located near the upper rim of the BAT, which probably originated from the BAT residual tissue and other adjacent tissues that include blood vessels and muscles.

It has been reported that BAT activation can be accomplished through Norepinephrine (NE) treatment and cold exposure [3,6]. First, we observed BAT activation with NE in the same group of mice with and without NE treatment under short (5 min) isoflurane anesthesia. The data showed significantly higher CLI signal under the NE-treated condition (1.23 fold) than without NE treatment (**Figure 3a**).

In human studies, PET imaging showed that subjects under cold exposure had much higher ^{18}F-FDG uptake in the BAT than those at room temperature [6]. In this mice study, a 39% increase in ^{18}F-FDG uptake was observed in the BAT of the animals treated with cold exposure (**Figure 3b**).

In mice, BAT activity can be influenced by different anesthesia regimens [3,41]. For example, ^{18}F-FDG uptake in BAT can be considerably decreased after one hour of anesthesia with ketamine [41]. Comparing the ^{18}F-FDG uptake in the same group of mice under short (5 min with isoflurane) and long anesthesia (70 min with ketamine/xylazine) regimens, a 54% decrease in ^{18}F-FDG BAT uptake was observed in the group anesthetized with ketamine/xylazine (**Figure 3c**).

It is well known that heme-containing proteins (such as hemoglobin in blood and cytochrome c in mitochondria) can lead to significant light absorption, and it is expected that the abundant blood vessels in BAT [1] will change the spectrum of CLI, and the spectral shape from the BAT area will be different from other areas. Conceivably, spectral unmixing techniques allow us to separate the two CLI spectra. From **Figure 4a**, no particular area was highlighted from the unmixed image of component #1 (Unmix #1), and the corresponding spectrum (blue line in **Figure 4d**) closely resembled the emission spectrum of ^{18}F in pure media, in which the CLI intensity is inversely correlated with the square of the wavelength [18,20]. This data suggests that Unmix #1 represented an unspecific CLI signal, which is probably from very shallow depths, such as ^{18}F-FDG accumulation in the skin. The peak of the unmixed #2 spectrum (red line) was around 640 nm, suggesting the signal was from the BAT. Interestingly, contrary to the significant attenuation of the intensity of CLI shorter than 640 nm, no dramatic decrease of intensity was observed once it reached its peak (red line in **Figure 4**), indicating better tissue penetration of the emitted light at longer wavelengths.

Multispectral Cerenkov luminescence tomography (msCLT) was used for the 3D reconstruction. msCLT has been previously reported by Kuo *et al.* [28,43], and is constructed from a set of 2D planar images acquired with a number of narrow bandpass filters (>5 filters). The reconstructed 3D images are coregistered with surface tomography that is generated from the structure light, and the images reveal that a substantial portion of the CLI signal originated from interscapular BAT (**Figure 5**). Remarkably, the coronal image (**Figure 5a**) clearly outlines the two lobes of BAT, which closely resemble the triangle contour of the BAT shown in **Figure 5e**.

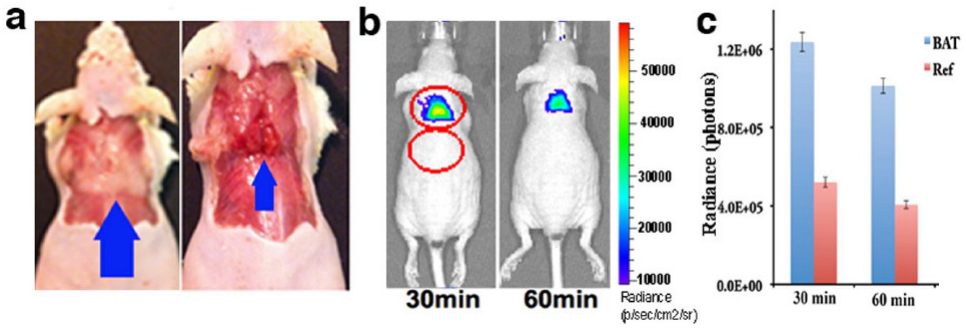

Figure 1: (**a**) Triangular contour of interscapular BAT (blue arrow) in a mouse; (left) BAT is covered with white adipose tissue, and (right) BAT is exposed. (**b**) CLI images of a mouse at 30 and 60 min after ^{18}F-FDG (280 µCi) intravenous injection. The images clearly outline the contour of BAT. (**c**) Quantitative analysis of CLI signal from interscapular BAT area and a reference area. Reprint from reference 42. Please click here to view a larger version of this figure.

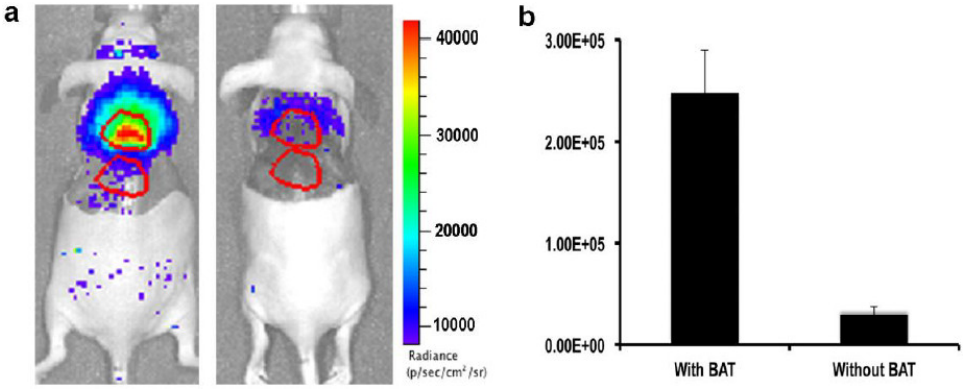

Figure 2: (**a**) Representative images of mice before (left) and after (right) BAT removal. (**b**) Quantification indicates that >85% CLI originated from BAT. Reprint from reference 42. Please click here to view a larger version of this figure.

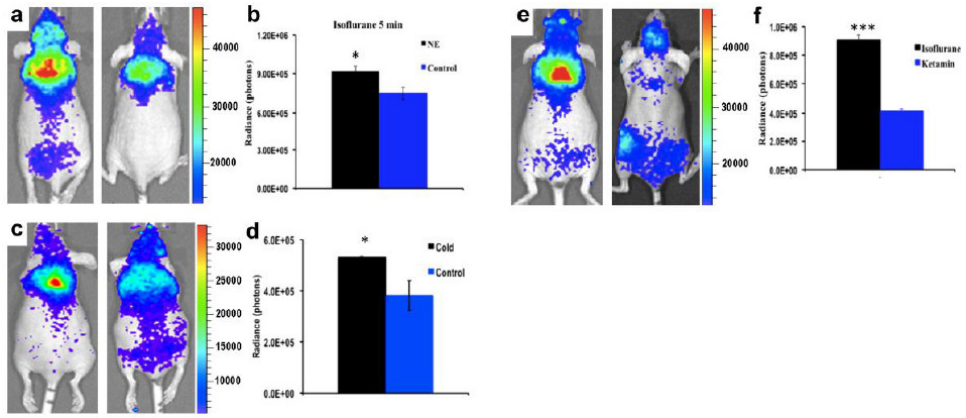

Figure 3: (**a**) Representative CLI images of BAT of mice with (left) and without (right) NE stimulation under short isoflurane anesthesia. (**b**) Quantitative analysis of the CLI signals from the two groups in (a) (n = 4 for each group). (**c**) Representative CLI images of BAT of mice with (left) and without (right) cold stimulation under short isoflurane anesthesia. (**d**) Quantitative analysis of the CLI signals from the two groups shown in (**e**) (n = 3 - 4 for each group). (**e**) Representative CLI images of BAT at 60 min after ^{18}F-FDG injection under short isoflurane anesthesia (5 min) (left) and ketamine/xylazine anesthesia (70 min) (right). (**f**) Quantitative analysis of the CLI signals from the two groups shown in (**g**) (n = 4 for each group). Reprint from reference 42. Please click here to view a larger version of this figure.

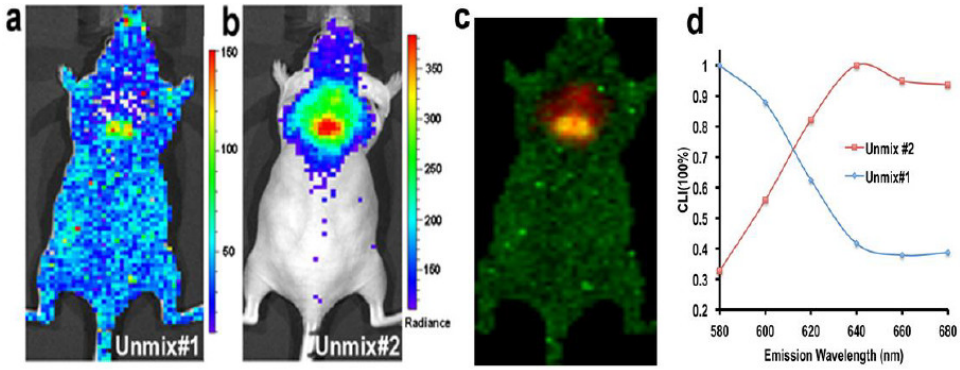

Figure 4: Spectral unmixing for unspecific CLI and BAT CLI. (**a**) Unmix #1 shows that unspecific CLI signal from ^{18}F-FDG is distributed over the whole body (the unmixed spectrum for this image is shown in (d) (blue line)). (**b**) Unmix #2 indicates that the majority of CLI at the interscapular site is from BAT (the unmixed spectrum is shown in (d) (red line)). The CLI peak is around 640 nm. (**c**) Merged image of Unmix #1 and #2. (**d**) The CLI spectra of Unmix #1 and #2. Reprint from reference 42. Please click here to view a larger version of this figure.

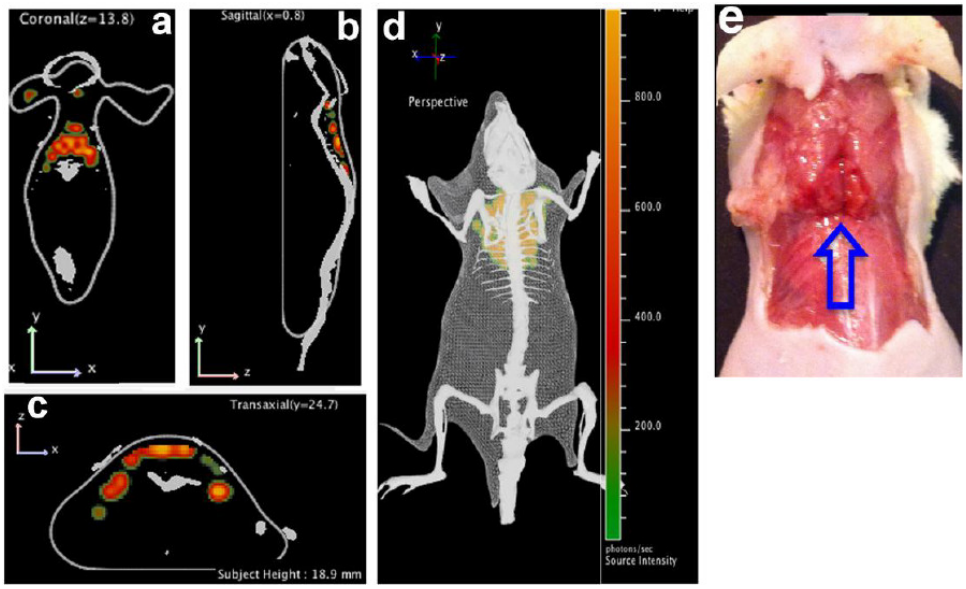

Figure 5: Multispectral Cerenkov luminescence tomography. (a - d) 3D reconstruction of the images. Interscapular BAT can be seen in coronal (**a**), sagittal (**b**), and transverse (**c**) views, as well as in the 3D image (**d**); (**e**) Physical BAT shape is shown (blue arrow) which correlates with reconstructed images. Reprint and adapt from reference 42. Please click here to view a larger version of this figure.

Discussion

Research related to BAT has been conducted for several decades. Previously, it had been considered to have no significant physiologic relevance during human adulthood [1]. However, recent large scale clinical PET imaging with ^{18}F-FDG and other investigations have confirmed BAT is still present in the upper chest, neck and other locations in adults [2,3]. Recent studies have strongly suggested that BAT plays an important role in obesity and diabetes [2,6]. Other research also indicates that BAT plays important roles during the process of ageing [12] and that its activity could be enhanced through exercise [10,44].

Both in clinical human studies and preclinical research, PET imaging with ^{18}F-FDG is the most used method to study BAT. However, for preclinical animal studies, PET is generally much more expensive than optical imaging. In this protocol, we demonstrate that CLI with ^{18}F-FDG can be applied for optically imaging BAT in small animals. Like other optical imaging techniques, tissue penetrating limitation and low sensitivity for deep targets are the intrinsic limitations of CLI [25,32]. Nonetheless, recently Spinelli *et al.* demonstrated that decent CLI signal could be observed with 10 mm tissue depth with ^{32}P [28,43], and Thorek *et al.* showed that 16 mm penetration could be achieved in lymph nodes of patients after ^{18}F-FDG injection [39,40]. Compared to PET imaging, CLI can be performed with a relatively low cost imaging system. Recently, Thorek *et al.* demonstrated that significantly high sensitivity could be achieved with CLI as low amounts of ^{18}F-FDG accumulated (about 2Ci) in the nodes of patients [39,40]. *In vitro* testing indicated that CLI signal from 0.01 Ci 90Y was detectable in solution [25,32,33]. Moreover, CLI also has the potential for high spatial resolution and the capacity for high throughput screening. In addition, CLI is easy to learn and use.

In the course of experiments, we found that CLI contrast of BAT with ^{18}F-FDG is highly related to the injection methods. Intravenous injection of ^{18}F-FDG can provide excellent contrast for interscapular BAT, while intraperitoneal injection with the same amount of ^{18}F-FDG only showed a weak contrast in the BAT area.

Spectral unmixing, a very practical technique to separate two sets of signals, has been widely used in fluorescence imaging. It is well known that the uptake of ^{18}F-FDG is not highly target-specific, and different targets/tissues have different light attenuation properties. We found the peak of the CLI spectrum of BAT is around 640 nm, and this data reflected the actual contexts of BAT. The 3D reconstruction of this protocol is very operable, because it can be performed with a commercially available optical imaging system based on the light diffusive properties of different wavelengths. With this approach, we can avoid the use of a specialized imaging system that requires multiple-angle view images for 3D reconstruction.

For both spectral unmixing and 3D reconstruction, a greater minimum of 600 photon counts from each image in BAT is required. To this end, large binning (bin = 16), small f stop (f = 1) and a long acquisition time (5 min) are needed for each image.

In summary, harnessing the unique location and shape of BAT and the significantly high uptake of ^{18}F-FDG in BAT, we demonstrate how BAT in small animals can be optically imaged with ^{18}F-FDG via the CLI technique. This method can be reliably used for imaging BAT and for monitoring BAT activation. Additionally, we also demonstrate that spectral unmixing and 3D reconstruction are practicable and 3D volume quantification is possible for future studies.

Disclosures

Publication of this video-article is supported by Perkin Elmer Company.

Acknowledgements

The authors thank Perkin Elmer Company for supporting this publication. We also thank Alana Ross, B.S. for proofreading this manuscript.

References

1. Cannon, B., & Nedergaard, J. Brown adipose tissue: function and physiological significance. *Physiol. Rev.* **84**, 277-359 (2004).
2. Cypess, A.M., *et al.* Identification and importance of brown adipose tissue in adult humans. *New Eng. J. Med.* **360**, 1509-1517 (2009).
3. Nedergaard, J., Bengtsson, T., & Cannon, B. Unexpected evidence for active brown adipose tissue in adult humans. *Amer. J. Physiol. Endocrinol. Metabolism.* **293**, E444-452 (2007).
4. Tseng, Y.H., *et al.* New role of bone morphogenetic protein 7 in brown adipogenesis and energy expenditure. *Nature.* **454**, 1000-1004 (2008).
5. Zhang, H., *et al.* Cross talk between insulin and bone morphogenetic protein signaling systems in brown adipogenesis. *Mol. Cell. Biol.* **30**, 4224-4233 (2010).
6. Marken Lichtenbelt, W.D., *et al.* Cold-activated brown adipose tissue in healthy men. *New Eng. J. Med.* **360**, 1500-1508 (2009).
7. Zingaretti, M.C., *et al.* The presence of UCP1 demonstrates that metabolically active adipose tissue in the neck of adult humans truly represents brown adipose tissue. *FASEB J.* **23**, 3113-3120 (2009).
8. Chen, Y.I., *et al.* Anatomical and Functional Assessment of Brown Adipose Tissue by Magnetic Resonance Imaging. *Obesity.* **20**, 1519-1526 (2012).
9. Chen, Y.C., *et al.* Measurement of human brown adipose tissue volume and activity using anatomic MR imaging and functional MR imaging. *J. Nucl. Med.* **54**, 1584-1587 (2013).
10. Bostrom, P., *et al.* A PGC1-alpha-dependent myokine that drives brown-fat-like development of white fat and thermogenesis. *Nature.* **481**, 463-468 (2012).
11. Yoneshiro, T., *et al.* Age-related decrease in cold-activated brown adipose tissue and accumulation of body fat in healthy humans. *Obesity.* **19**, 1755-1760 (2011).
12. Mattson, M.P. Perspective: Does brown fat protect against diseases of aging? *Ageing Res. Rev.* **9**, 69-76 (2010).
13. Stephens, M., Ludgate, M., & Rees, D.A. Brown fat and obesity: the next big thing? *Clin. endocrinol.* **74**, 661-670 (2011).
14. Harms, M., & Seale, P. Brown and beige fat: development, function and therapeutic potential. *Nat. Med.* **19**, 1252-1263 (2013).
15. Farmer, S.R. Obesity: Be cool, lose weight. *Nature.* **458**, 839-840 (2009).
16. Inokuma, K., *et al.* Uncoupling protein 1 is necessary for norepinephrine-induced glucose utilization in brown adipose tissue. *Diabetes.* **54**, 1385-1391 (2005).
17. Isler, D., Hill, H.P., & Meier, M.K. Glucose metabolism in isolated brown adipocytes under beta-adrenergic stimulation. Quantitative contribution of glucose to total thermogenesis. *Biochem. J.* **245**, 789-793 (1987).
18. Robertson, R., *et al.* Optical imaging of Cerenkov light generation from positron-emitting radiotracers. *Phys. Med. Biol.* **54**, N355-365 (2009).
19. Spinelli, A.E., *et al.* Cerenkov radiation allows in vivo optical imaging of positron emitting radiotracers. *Phys. Med. Biol.* **55**, 483-495 (2010).
20. Liu, H., *et al.* Molecular optical imaging with radioactive probes. *PloS One.* **5**, e9470 (2010).
21. Ran, C., Zhang, Z., Hooker, J., & Moore, A. In vivo photoactivation without 'light': use of Cherenkov radiation to overcome the penetration limit of light. *Mol. Imaging. Biol.* **14**, 156-162 (2012).
22. Dothager, R.S., Goiffon, R.J., Jackson, E., Harpstrite, S., & Piwnica-Worms, D. Cerenkov radiation energy transfer (CRET) imaging: a novel method for optical imaging of PET isotopes in biological systems. *PloS One.* **5**, e13300 (2010).
23. Ruggiero, A., Holland, J.P., Lewis, J.S., & Grimm, J. Cerenkov luminescence imaging of medical isotopes. *J. Nucl. Med.* **51**, 1123-1130 (2010).
24. Lewis, M.A., Kodibagkar, V.D., Oz, O.K., & Mason, R.P. On the potential for molecular imaging with Cerenkov luminescence. *Optics Letters.* **35**, 3889-3891 (2010).
25. Mitchell, G.S., Gill, R.K., Boucher, D.L., Li, C., & Cherry, S.R. In vivo Cerenkov luminescence imaging: a new tool for molecular imaging. *Philosophical transactions. Series A, Mathematical, physical, and engineering sciences.* **369**, 4605-4619 (2011).
26. Thorek, D.L., Ogirala, A., Beattie, B.J., & Grimm, J. Quantitative imaging of disease signatures through radioactive decay signal conversion. *Nat. Med.* **19**, 1345-1350 (2013).

27. Holland, J.P., Normand, G., Ruggiero, A., Lewis, J.S., & Grimm, J. Intraoperative imaging of positron emission tomographic radiotracers using cerenkov luminescence emissions. *Mol. Imaging.* **11**, 1-10 (2012).
28. Spinelli, A.E.*, et al.* Multispectral Cerenkov luminescence tomography for small animal optical imaging. *Optics Express* **19**, 12605-12618 (2011).
29. Xu, Y.*, et al.* Proof-of-concept study of monitoring cancer drug therapy with cerenkov luminescence imaging. *J. Nucl. Med.* **53**, 312-317 (2012).
30. Liu, H.*, et al.* Intraoperative imaging of tumors using cerenkov luminescence endoscopy: a feasibility experimental study. *J. Nucl. Med.* **53**, 1579-1584 (2012).
31. Thorek, D.L.*, et al.* Positron lymphography: multimodal, high-resolution, dynamic mapping and resection of lymph nodes after intradermal injection of 18F-FDG. *J. Nucl. Med.* **53**, 1438-1445 (2012).
32. Xu, Y., Liu, H., & Cheng, Z. Harnessing the power of radionuclides for optical imaging: Cerenkov luminescence imaging. *J. Nucl. Med.* **52**, 2009-2018 (2011).
33. Spinelli, A.E., Marengo, M., Calandrino, R., Sbarbati, A., & Boschi, F. Optical imaging of radioisotopes: a novel multimodal approach to molecular imaging. *Quart. J. Nucl. Med. Mol. Imaging.* **56**, 280-290 (2012).
34. Hu, Z.*, et al.* Experimental Cerenkov luminescence tomography of the mouse model with SPECT imaging validation. *Optics Express* **18**, 24441-24450 (2010).
35. Hu, Z.*, et al.* Cerenkov luminescence tomography of aminopeptidase N (APN/CD13) expression in mice bearing HT1080 tumors. *Mol. Imag.* **12**, 173-181 (2013).
36. Zhong, J.*, et al.* Cerenkov luminescence tomography for in vivo radiopharmaceutical imaging. *Internatl. J. Biomed. Imaging.* **2011**, 641618 (2011).
37. Zhong, J., Qin, C., Yang, X., Chen, Z., & Tian, J. Fast-specific tomography imaging via Cerenkov emission. *Mol. Imaging. Biol.* **14**, 286-292 (2012).
38. Kothapalli, S.R., Liu, H., Liao, J.C., Cheng, Z., & Gambhir, S.S. Endoscopic imaging of Cerenkov luminescence. *Biomed. Optics Express.* **3**, 1215-1225 (2012).
39. Spinelli, A.E.*, et al.* First human Cerenkography. *J. Biomed. optics.* **18**, 20502 (2013).
40. Thorek, D.L., Riedl, C., & Grimm, J. Clinical Cerenkov Luminescence Imaging of 18F-FDG. *J. Nucl. Med.* **55,** 1345-50 (2014).
41. Fueger, B.J.*, et al.* Impact of animal handling on the results of 18F-FDG PET studies in mice. *J. Nucl. Med.* **47**, 999-1006 (2006).
42. Zhang, X., Kuo, C., Moore, A., & Ran, C. In vivo optical imaging of interscapular brown adipose tissue with (18)F-FDG via Cerenkov luminescence imaging. *PloS One.* **8**, e62007 (2013).
43. Kuo, C., Coquoz, O., Troy, T.L., Xu, H., & Rice, B.W. Three-dimensional reconstruction of in vivo bioluminescent sources based on multispectral imaging. *J. Biomed. Optics.* **12**, 024007 (2007).
44. Xu, X.*, et al.* Exercise ameliorates high-fat diet-induced metabolic and vascular dysfunction, and increases adipocyte progenitor cell population in brown adipose tissue. *Amer. J. Physiol. Regulatory, integrative and comparative physiology.* **300**, R1115-1125 (2011).